Towards Optimal Aggregation of Varying Range Dependencies in Haze Removal

Xiaozhe Zhang Fengying Xie Haidong Ding Linpeng Pan Zhenwei Shi Beihang University

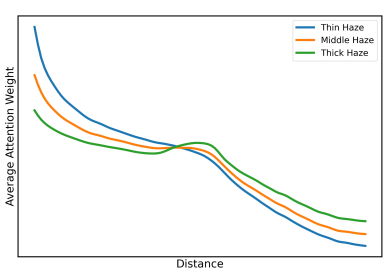
Abstract

Haze removal aims to restore a clear image from a hazy input. Existing methods have shown significant efficacy by capturing either short-range dependencies for local detail preservation or long-range dependencies for global context modeling. Given the complementary strengths of both approaches, a intuitive advancement is to explicitly integrate them into a unified framework. However, this potential remains underexplored in current research. In this paper, we propose DehazeMatic, which leverages the proposed Transformer-Mamba Dual Aggregation block to simultaneously and explicitly captures both short- and longrange dependencies through dual-path design for improved restoration. To ensure that dependencies at varying ranges contribute optimally to performance, we conduct extensive experiments to identify key influencing factors and determine that an effective aggregation mechanism should be guided by the joint consideration of haze density and semantic information. Building on these insights, we introduce the CLIP-enhanced Dual-path Aggregator, which utilizes the rich semantic priors encapsulated in CLIP and the estimated haze density map, derived from its powerful generalization ability, to instruct the aggregation process. Extensive experiments demonstrate that DehazeMatic outperforms sort-of-the-art methods across various benchmarks.

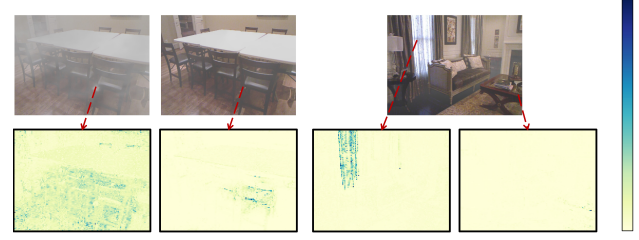
1. Introduction

Single image dehazing aims to recover a clear image from a hazy input, serving as a crucial pre-processing step for high-level vision tasks under hazy conditions, such as object detection [39] and semantic segmentation [53].

Current data-driven methods can be categorized into two classes based on the receptive field size of the operators used for feature extraction, namely (*i*) using convolution [5, 7, 13, 37, 55, 56, 72] or window-based self-attention [35, 34, 59, 64] and (*ii*) using linear self-attention [51] or State Space Model (SSM) [58, 80, 73]. The former excels at capturing short-range dependencies but lacks effective global modeling capabilities [30, 62, 12]. In contrast, the latter directly models long-range dependencies while ensuring efficient computation; however, it fails to preserve local 2D



(a) Quantitative presentation of haze density influencing the required dependencies.

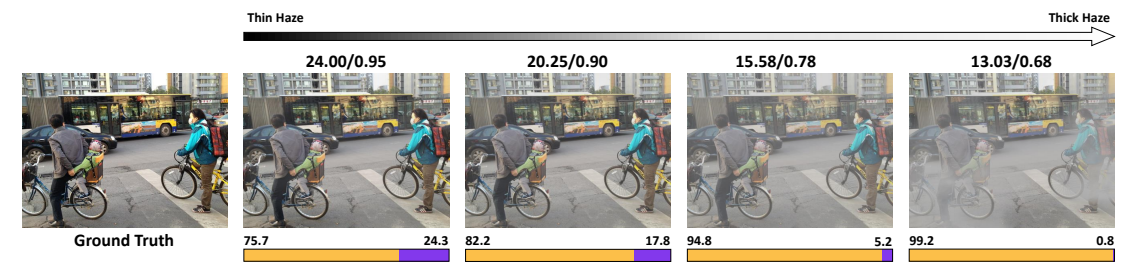


(b) Qualitative presentation of haze density (left) and semantic information (right) influencing the required dependencies.

Figure 1. Illustration of factors influencing the relative importance between short-range and long-range dependencies. We train a Transformer-based dehazing network with a global receptive field and synthesis hazy images with different densities based on the Atmospheric Scattering Model [49]. (a) The horizontal axis represents the Euclidean distance between the current token and all other tokens, while the vertical axis represents the average attention weights between the current token and all tokens at the corresponding distance. The curve data is derived from all tokens of all images in the test set. (b) The bottom visualizes the attention map between the chosen tokens (indicated by the tails of red arrows) and all other tokens. On the left is the visualization of tokens at the same position corresponding to the same ground truth image, but with different haze densities. On the right is a visualization of tokens with different semantic information on the same homogeneous haze image. More analysis is in supplementary material.

inductive bias [25, 14].

Both categories of methods have achieved excellent performance, and their respective strengths can address the limitations of the other. Therefore, a natural idea is that explicitly combining short- and long-range dependencies (*i.e.*, leveraging the strengths of both approaches) is expected to yield even more promising results. However, this integration has not been well explored. To address this gap, we will employ a dual-path design that concurrently captures



Prompts: ['A hazy image.', 'A clear image.']

Figure 2. Illustration of CLIP [52]'s potential to perceive haze and its density. We use the ViT-B/32 OpenCLIP [26] model, pre-trained on the LAION dataset, for our experiments. The values above the images indicate the PSNR and SSIM metrics, which reflect haze density from a quantitative perspective. The values below the images represent the similarity scores between the images and the paired prompts from CLIP. Notably, as haze density increases, the similarity score with the haze-describing prompt also increases.

fine-grained perception from nearest neighbor features and holistic contextual cues from non-local relationships. The ensuing problem is that reasonably integrating short- and long-range dependencies from these two paths is a non-trivial task, because tokens with different characteristics in the image require varying ranges of dependencies. Simple addition or concatenation often leads to suboptimal performance. More importantly, there is still no clear guidance on how to determine the relative importance between short-range and long-range dependencies for each token.

One preliminary hypothesis is that haze density serves as a determining factor. To verify this, we conduct an experiment. As shown in Figure 1(a), higher haze density increases reliance on long-range dependencies, whereas lower haze density requires more short-range dependencies. Furthermore, additional investigation reveals that tokens with varying semantic information require different ranges of dependencies, as illustrated on the right side of Figure 1(b). Based on these findings, we conclude that haze density and semantic information jointly determine the relative importance of short-range and long-range dependencies.

In this paper, building on the above insights, we propose **DehazeMatic**, where *M*amba and *T*ransformer are *I*ntegrated by *C*LIP for image *dehazing*. The core building block of the DehazeMatic is the proposed *Trans*former-Mamba Dual Aggregation (TrambaDA) block, which employs a dual-path design. In one path, we utilize window-based self-attention [45] to capture short-range dependencies. In the other path, inspired by recent advances in SSMs [18, 19, 44, 82, 42], we incorporate the Selective Scan Space State Sequential Model (S6) block [18], which maintains global information indefinitely with linear complexity. We also adopt the four-way scanning strategy to mitigate the "direction-sensitive" problem caused by the non-causal nature of visual data [44].

Next, to ensure that both short- and long-range dependencies contribute optimally to performance, a dual-path aggregator capable of adaptively learning the relative importance of each path is required. As indicated by Figure 1, the aggregator must capture both the haze density and se-

mantic information of each token in the input image. Recent advances in CLIP [52], pre-trained on web-scale datasets, reveal that it not only encapsulates rich semantic priors (e.g., enabling strong performance in zero-shot semantic segmentation [81, 76]), but also has the potential to perceive haze and its density (as shown in Figure 2). Motivated by this, we propose the CLIP-enhanced Dual-path Aggregator (CedA). Specifically, we treat the affinity scores between the the patch-wise image embeddings from the CLIP image encoder and the text embeddings of paired prompts describing clear and hazy conditions from the CLIP text encoder as the estimated haze density map. To find the best prompts for better estimation and avoid labor-intensive prompt engineering, these paired prompts are learned. For semantic information, we reuse the patch-wise image embeddings to provide high-level and abstract features while avoiding additional computational overhead. To supplement the lowlevel details, we incorporate the input features from the TrambaDA blocks and align both representations using a bidirectional cross-attention mechanism. Finally, we generate dual-path aggregation weights based on the refined semantic information and the estimated haze density map.

Our contributions can be summarized as follows:

- We propose DehazeMatic, which demonstrates the superiority of explicitly and simultaneously capturing both short- and long-range dependencies while effectively aggregating dependencies across varying ranges. It achieves SOTA performance in various benchmarks.
- For the first time, we identify the key factors required for reasonably aggregating dependencies across different ranges in image dehazing. Based on these insights, we propose the CedA module, which performs dynamic aggregation according to haze density and semantic characteristics of each token within the image.
- The proposed CedA module further explore the potential of CLIP in image dehazing and, for the first time, demonstrate its capability in haze density estimation, all without the need for fine-tuning the encoder.

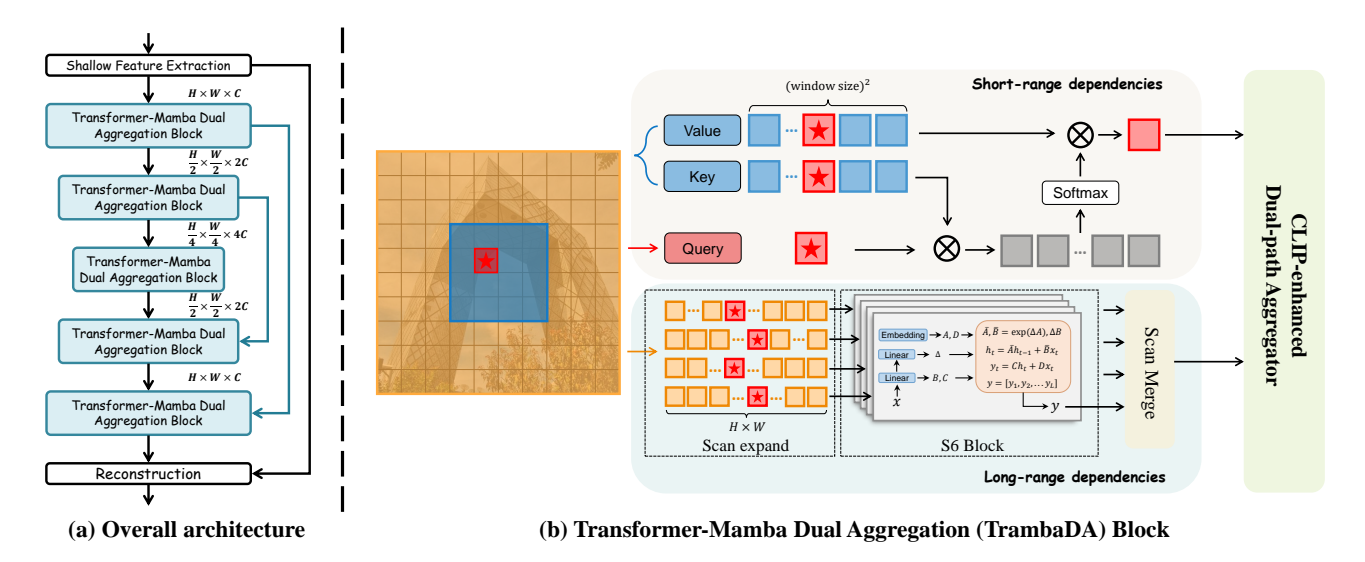


Figure 3. (a) The architecture of our proposed DehazeMatic. (b) The inner structure of Transformer-Mamba Dual Aggregation (TrambaDA) block. The weights generated by CLIP-enhanced Dual-path Aggregator (CedA) are used to aggregate the outputs of dual-path.

2. Related Work

2.1. Single Image Dehazing

Due to spatially variant transmission map and atmospheric light, single image dehazing is a highly ill-posed problem. Early prior-based methods [23, 16, 31, 60, 83, 6] achieved dehazing by imposing various assumptions to estimate key parameters in the Atmospheric Scattering Model (ASM) [49]. ASM provides strong theoretical support and interpretability for these methods; however, they often fail when images deviate from statistical laws.

With the rapid advancement of deep learning [33], numerous learning-based methods have been proposed, resulting in improved performance. Early methods [7, 37] employ neural networks to estimate key parameters in the ASM and subsequently restore the haze-free images. Later, ASM-independent deep networks [54, 55, 43, 40, 57, 13, 75, 50, 36, 66, 70, 59, 17, 68, 77, 8, 15, 9, 65, 69, 11] directly estimate clear images or haze residuals. hazeFormer [59] is a representative method that achieves efficient feature extraction through window-based selfattention and several key modifications. However, its inherently limited receptive field constrains its performance potential. To achieve a global receptive field with lower computational overhead, some methods [58, 71] incorporate frequency domain features into image dehazing, offering the additional benefit of more direct learning of highfrequency information. For the same purpose, other researchers [79, 73] introduce the Mamba [18] architecture into image dehazing. However, none of these methods address how to better integrate global semantic features with local texture features.

2.2. CLIP for Low-Level Vision Tasks

Classic vision-language models, such as CLIP [52], aim to learn aligned features in the embedding space from image-text pairs using contrastive learning. Some studies have explored leveraging the rich prior knowledge encapsulated in CLIP to assist with low-level vision tasks.

In All-in-One image restoration, some researchers [47, 1, 27] use degradation embeddings from the CLIP image encoder to implicitly guide the network in making adaptive responses. In monocular depth estimation, recent studies [74, 4, 24] use CLIP to map patches of the input image to specific semantic distance tokens, which are then projected onto a quantified depth bin for estimation. In low-light enhancement, some methods [41, 48] use text-image similarity between the enhanced results and learnable prompt pairs to train the enhancement network.

Some works also introduce CLIP into image [63] and video [53] dehazing, but they all use text-image similarity between dehazed results and contrastive prompt sets as regularization to guide the restoration process. In contrast, our method further exploits the potential of CLIP by directly incorporating its latent embeddings into the main network to guide the dehazing process.

3. Method

3.1. Overall Architecture

The architecture of DehazeMatic is depicted in Figure 3. Given a hazy image, shallow features are first extracted and then passed through a symmetric encoder-decoder framework. Each stage of encoder and decoder consists of multiple Transformer-Mamba Dual Aggregation (TrambaDA)

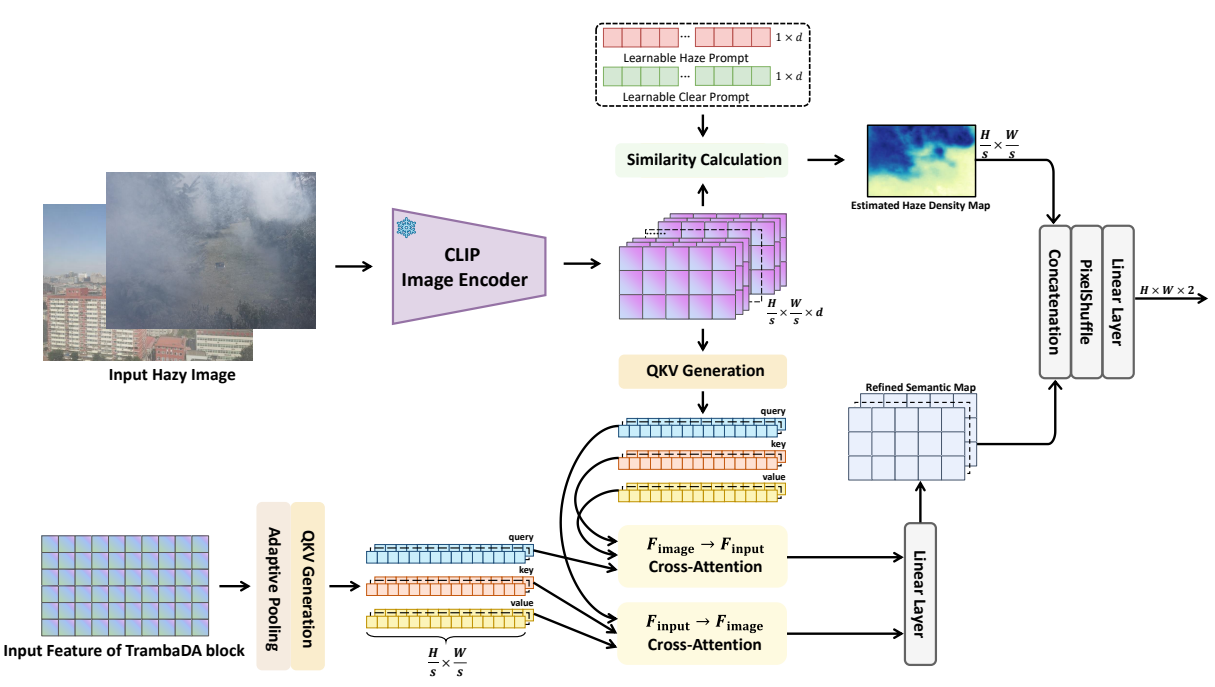


Figure 4. Illustration of the CLIP-enhanced Dual-path Aggregator generating aggregation weights. To ensure computational efficiency, the TrambaDA blocks share the same aggregation weights at each stage.

blocks, along with corresponding downsampling or upsampling operations. We also incorporate skip connections between the encoder and decoder at each level. Finally, the output of the last decoder stage is combined with the input hazy image to produce the haze-free image.

3.2. Transformer-Mamba Dual Aggregation Block

The TrambaDA block's backbone employs a dual-path design, with one path capturing short-range dependencies and the other capturing long-range dependencies, thereby providing complementary restoration information for image tokens with distinct characteristics.

Capturing Short-range Dependencies. We construct this path using window-based self-attention [45], which offers stronger fitting capability through dynamic weights. Specifically, given the input feature $F_{\rm in} \in \mathbb{R}^{H \times W \times C}$, we first divide $F_{\rm in}$ into non-overlapping windows with size of $M \times M$, then obtain flattened feature $F_{\rm in}^i \in \mathbb{R}^{M^2 \times C}$ of each window i. For simplicity, we only consider the single-head attention. Performing self-attention on non-overlapping windows can be formulated as:

$$\begin{split} F_{\text{out_short}}^{i} = & \text{Attention}(F_{\text{in}}^{i}W^{Q}, F_{\text{in}}^{i}W^{K}, F_{\text{in}}^{i}W^{V}), \\ & \text{Attention}(Q, K, V) = \text{Softmax}(\frac{QK^{T}}{\sqrt{d_{k}}})V, \\ & F_{\text{out_short}} = & \{F_{\text{out_short}}^{1}, F_{\text{out_short}}^{2}, \cdots, F_{\text{out_short}}^{N}\}, \end{split} \tag{1}$$

where $N = HW/M^2$; $W^Q, W^K, W^V \in \mathbb{R}^{C \times d_k}$ are projection matrices for queries, keys, and values, respectively.

Capturing Long-range Dependencies. We build this path using Mamba [18]'s S6 block, which preserves the global receptive field with linear complexity and incorporates hardware-aware algorithms.

Due to the "direction-sensitive" problem caused by the non-causal nature of visual data, directly applying the S6 block on the flattened image will result in suboptimal performance [44]. Following Vmamba [44], we unfold feature map along four directions, generating four independent sequences. Each feature sequence is processed through the S6 block, and all output sequences are merged into a new sequence. This process can be represented as follows:

$$F_{\rm in}^d = expand(F_{\rm in}, d), d = \{1, 2, 3, 4\},$$

$$\bar{F}_{\rm in}^d = \text{S6}(F_{\rm in}^d), \qquad (2)$$

$$F_{\rm out,long} = merge(\bar{F}_{\rm in}^1, \bar{F}_{\rm in}^2, \bar{F}_{\rm in}^3, \bar{F}_{\rm in}^4),$$

where $expand(\cdot)$ and $merge(\cdot)$ correspond to the *scan expand* and *scan merge* operations, respectively.

3.3. CLIP-enhanced Dual-path Aggregator

The CLIP-enhanced Dual-path Aggregator (CedA) utilizes the generated pixel-level weights to adaptively aggregate dual-path outputs, ensuring that dependencies across varying ranges contribute optimally to performance:

$$F_{out} = W_{short} F_{out_short} + W_{long} F_{out_long}.$$
 (3)

 $W_{short}, W_{long} \in \mathbb{R}^{H \times W}$ are the aggregation weights corresponding to short- and long-range dependencies, respec-



Figure 5. Illustration of estimated haze density maps. The proposed method can identify the relative haze density not only in different regions of non-homogeneous haze images but also between two homogeneous haze images.

tively, and their generation process is shown in Figure 4.

3.3.1 Estimating Haze Density Map

Define Estimation Pipeline. Inspired by Figure 2, we leverage CLIP to estimate the haze density map. Specifically, given a hazy image $I_{\text{haze}} \in \mathbb{R}^{H \times W \times 3}$ and a paired prompts describing haze and clear conditions $T = [T_{\text{haze}}, T_{\text{clear}}]$ (e.g., ['hazy image', 'clear image']), we encode them into latent space using a pretrained CLIP model:

$$F_{\text{image}} = \Phi_{\text{image}}(I_{\text{haze}}) \in \mathbb{R}^{H_p \times W_p \times d_c},$$

$$F_{\text{text}} = \Phi_{\text{text}}(T) \in \mathbb{R}^{2 \times d_c},$$
(4)

where $\Phi_{\rm text}$ is the CLIP text encoder, and $\Phi_{\rm image}$ is the CLIP image encoder without the final pooling layer, allowing the generation of a patch-wise density map. H_p and W_p denote the height and width of the encoded image embedding, respectively, while d_c denotes the hidden dimension of CLIP. As shown in Figure 2, as the haze density increases, the similarity scores between $F_{\rm image}$ and the haze-describing prompt $T_{\rm haze}$ also increase. Therefore, we treat these similarity scores as the estimated density map \mathcal{M}_d :

$$\mathcal{M}_d = \text{Softmax}(\text{sim}(F_{\text{image}}, F_{\text{text}}))[:, :, 0],$$
 (5)

where $sim(\cdot, \cdot)$ is the similarity calculation, and final haze density map $\mathcal{M}_d \in \mathbb{R}^{H_p \times W_p}$.

Train Learnable Haze/Clear Prompts. To find the best prompts for improved estimation and avoid time-consuming prompt engineering, we use learnable prompt tokens instead of manually predefined prompts to describe abstract haze and clear conditions.

The training process consists of two stages. In the first stage, we optimize the learnable paired prompts using cross-entropy loss, enabling them to preliminarily distinguish between haze and clear conditions. Given a hazy and clear image $I_{\text{haze}}, I_{\text{clear}} \in \mathbb{R}^{H \times W \times 3}$, we define the

first-stage loss \mathcal{L}_1 as:

$$\mathcal{L}_{1} = -(y * \log(\hat{y}) + (1 - y) * \log(1 - \hat{y})),$$

$$\hat{y} = \frac{e^{\cos(\text{Pool}(\Phi_{\text{image}}(I)), \Phi_{\text{text}}(T_{\text{clear}}))}}{\sum_{i \in \{\text{haze, clear}\}} e^{\cos(\text{Pool}(\Phi_{\text{image}}(I)), \Phi_{\text{text}}(T_{i}))}},$$
(6)

where $I \in \{I_{\text{haze}}, I_{\text{clear}}\}$ and y is the label of the current image, 0 is for hazy image I_{haze} and 1 is for clear image I_{clear} . Since Φ_{image} is the CLIP image encoder without the final pooling layer, we apply a global pooling layer Pool() to obtain the latent image embedding with a shape of $\mathbb{R}^{1 \times d_c}$.

In the second stage, our goal is to achieve better prediction of haze density. The most straightforward and effective optimization approach is regression. However, there is no ground-truth density map corresponding to the hazy image in the existing dataset. To address this, we construct triplet data $\{I_{\rm haze}, I_{\rm clear}, I_{\rm density}\}$ based on Atmospheric Scattering Model [49]. The second-stage loss \mathcal{L}_2 is defined as:

$$\mathcal{L}_2 = \begin{cases} \alpha_1 \text{MSE}(\mathcal{M}_d, I_{\text{density}}) + \alpha_2 \mathcal{L}_1, & y = 0\\ \mathcal{L}_1, & y = 1 \end{cases}$$
 (7)

where MSE() is the mean absolute error, and \mathcal{M}_d is obtained from I_{haze} and the learnable paired prompts $T = [T_{\text{haze}}, T_{\text{clear}}]$ according to Equation 5. α_1 and α_2 are the weights of different loss functions. More details is in supplementary material. Training is lightweight since there is no need to fine-tune the CLIP image encoder.

Finally, we use the learned paired prompts $[T_{\rm haze}, T_{\rm clear}]$ to generate the estimated patch-wise haze density map \mathcal{M}_d . Some examples are shown in Figure 5, demonstrating that our method is an effective and universal approach applicable to both homogeneous and non-homogeneous haze.

3.3.2 Obtaining Refined Semantic Map

Considering that the pretrained image encoder of CLIP is obtained through a classification pretext task, each location in the feature map before pooling captures regional semantic information [74]. Therefore, we reuse $F_{\rm image}$ from

Table 1. Quantitative comparisons of various methods on various dehazing benchmarks. The best results and the second best results are in **bold** and <u>underline</u>, respectively.

			RESIDE	E SOTS (He	omogeneo	us Haze)		N	on-homog	eneous Ha	ze	Over	haad
Methods	Publication	Outo	loor	Ind	oor	Ave	rage	NH-	Haze	Dense	-Haze	Over	nead
		PSNR↑	SSIM↑	PSNR↑	SSIM↑	PSNR↑	SSIM↑	PSNR↑	SSIM↑	PSNR↑	SSIM↑	#Param	MACs
DCP [22]	TPAMI-10	19.14	0.861	16.61	0.855	17.88	0.858	10.57	0.520	10.06	0.385	-	-
AOD-Net [37]	ICCV-17	24.14	0.920	20.51	0.816	22.33	0.868	15.40	0.569	13.14	0.414	1.76K	0.12G
GridDehazeNet [43]	ICCV-19	30.86	0.982	32.16	0.984	31.51	0.983	18.33	0.667	14.96	0.533	0.96M	21.55G
FFA-Net [50]	AAAI-20	33.57	0.984	36.39	0.989	34.98	0.987	19.87	0.692	16.09	0.503	4.46M	288.86G
DeHamer [20]	CVPR-22	35.18	0.986	36.63	0.988	35.91	0.987	20.66	0.684	16.62	0.560	132.45M	59.25G
SRDefog [28]	ACCV-22	-	-	-	-	-	-	20.99	0.610	16.67	0.500	12.56M	24.18M
MAXIM-2S [61]	CVPR-22	34.19	0.985	38.11	0.991	36.15	0.988	-	-	-	-	14.10M	216.00G
SGID-PFF [5]	TIP-22	30.20	0.975	38.52	0.991	34.36	0.983	-	-	-	-	13.87M	156.67G
PMNet [70]	ECCV-22	34.74	0.985	38.41	0.990	36.58	0.988	20.42	0.730	16.79	0.510	18.90M	81.13G
MB-TaylorFormer-B [51]	ICCV-23	37.42	0.989	40.71	0.992	39.07	0.991	-	-	16.66	0.560	2.68M	38.50G
MITNet [58]	MM-23	35.18	0.988	40.23	0.992	37.71	0.990	21.26	0.712	<u>16.97</u>	0.606	2.73M	16.42G
DehazeFormer [59]	TIP-23	34.29	0.983	38.46	0.994	36.38	0.989	20.31	0.761	16.66	0.595	4.63M	48.64G
SCANet [21]	CVPR-23	-	-	-	-	-	-	19.52	0.649	15.35	0.508	2.39M	258.63G
DEANet [8]	TIP-24	36.03	0.989	40.20	0.993	38.12	0.991	20.84	0.801	16.73	0.602	3.65M	32.23G
UVM-Net [79]	Arxiv-24	34.92	0.984	40.17	0.996	37.55	0.990	-	-	-	-	19.25M	173.55G
OKNet [10]	AAAI-24	35.45	0.992	37.59	0.994	36.52	0.993	20.29	0.800	16.85	0.620	4.42M	39.54G
DCMPNet [77]	CVPR-24	36.56	0.993	42.18	0.996	39.37	0.995	-	-	-	-	18.59M	80.42G
DehazeMatic	-	38.21	0.995	41.50	0.996	39.86	0.996	21.47	0.806	17.28	0.629	4.58M	35.50G

Equation 4 and regard it as semantic information. This approach not only provides high-level information but also avoids introducing additional computational overhead.

However, relying solely on F_{image} leads to suboptimal performance, primarily because it is an abstract representation and lacks low-level semantic details. To address this limitation, we incorporate the input features of the TrambaDA blocks, F_{input} , to supplement F_{image} and introduce a bidirectional cross-attention mechanism to align their semantic information across different scales, thereby yielding a refined semantic map \mathcal{M}_s :

$$\mathcal{M}_{s} = \operatorname{Linear}(\operatorname{Attention}_{\operatorname{input} \to \operatorname{image}}(Q_{image}, K_{input}, V_{input}),$$

$$(\operatorname{Attention}_{\operatorname{image} \to \operatorname{input}}(Q_{input}, K_{image}, V_{image})).$$
(8)

 Q_i , K_i and V_i represent the query, key, and value derived from F_i after channel reduction or adaptive pooling, where $i \in \{\text{image, input}\}$. This process is shown in Figure 4.

3.3.3 Generating Dual-path Aggregation Weights

Finally, the estimated haze density map \mathcal{M}_d and the obtained refined semantic map \mathcal{M}_s are jointly used to generate the dual-path aggregation weights, as follows:

$$W_{short}, W_{long} = \text{Split}(\text{Linear}(\text{Interpolate}(\text{Concat}(\mathcal{M}_d, \mathcal{M}_s)))).$$
 (9)

Here, $\operatorname{Concat}(\cdot)$ denotes a concatenation operation, $\operatorname{Interpolate}(\cdot)$ represents an interpolation operation used to resize \mathcal{M}_d and \mathcal{M}_s to match the dimensions of $F_{\operatorname{out_short}}$ and $F_{\operatorname{out_long}}$, $\operatorname{Linear}(\cdot)$ refers to a projection layer, and $\operatorname{Split}(\cdot)$ indicates a channel-wise splitting operation. The aggregation is subsequently performed using Equation 3.

4. Experiments

4.1. Experiment Setup

Training Details. DehazeMatic is implemented with Py-Torch on NVIDIA A100 GPUs. We use Adam [32] optimizer with default parameters ($\beta_1=0.9,\ \beta_2=0.99$) and a cosine annealing strategy [46] with restarts. The initial learning rate is set to 2×10^{-4} , gradually decreasing to 2×10^{-6} . We train the homogeneous haze dataset for 200 epochs and the non-homogeneous haze dataset for 400 epochs. The images are randomly cropped to a size of 256×256 and augmented with flipping. We use L1 and perceptual loss [29] to supervise dehazing process.

Datasets. We evaluate the proposed DehazeMatic on homogeneous (*i.e.*, RESIDE [38]) and non-homogeneous haze datasets (*i.e.*, NH-HAZE [3] and Dense-Haze [2]). The RESIDE [38] includes two training subsets: the Indoor Training Set (ITS) with 13,990 pairs of indoor images, and the Outdoor Training Set (OTS) with 313,950 pairs of outdoor images. Models are evaluated on the corresponding subset of the Synthetic Objective Testing Set (SOTS). The NH-HAZE [3] and Dense-Haze [2] use a professional haze generator to simulate real hazy conditions, making them suitable for evaluating model performance in real-world non-homogeneous haze removal. These datasets contain 55 and 55 paired images, respectively. We use the last 5 images as the testing set and the remaining images as the training set.

4.2. Comparison with SOTA Methods

Table 1 shows the quantitative results on various benchmarks. As the parameters of the CLIP encoder are frozen,

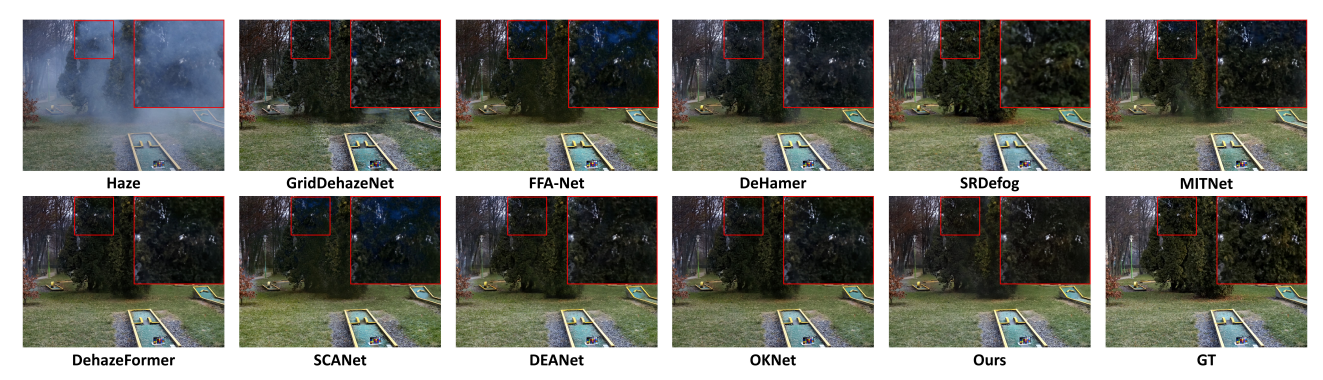


Figure 6. Visual comparisons on the NH-Haze dataset [3]. The red boxes highlight the restoration effects for thick haze and texture details. Please zoom in for the best view.

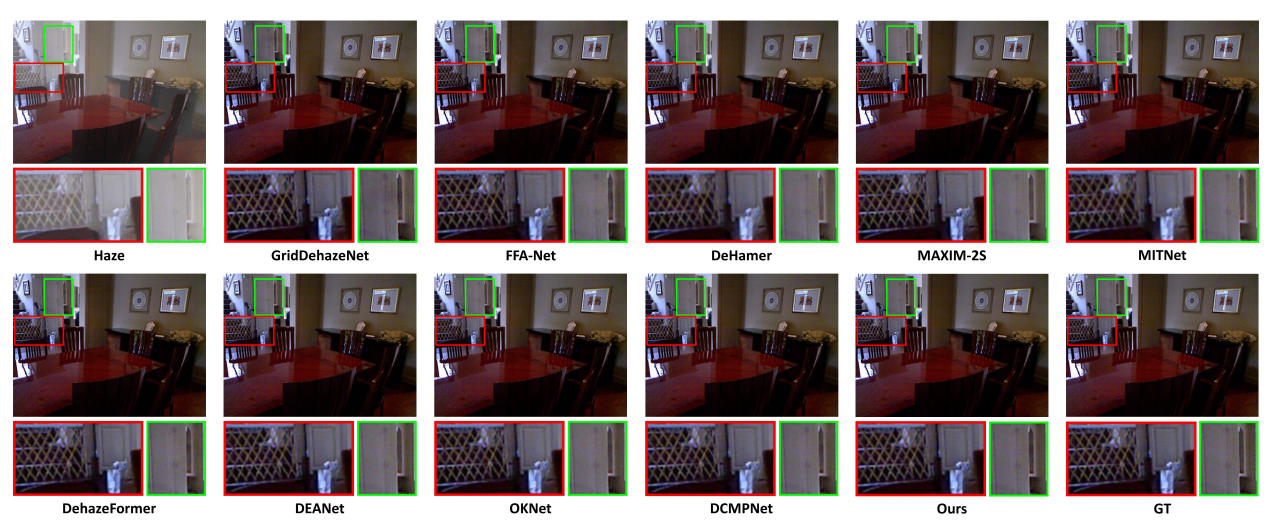


Figure 7. Visual comparisons on RESIDE SOTS Indoor dataset [38]. The red boxes and green boxes show the restoration of high-frequency and low-frequency information, respectively.

we exclude them from the overhead, which is consistent with previous work. Notably, the additional inference time introduced by CLIP is minimal, requiring only 3.8 ms per image on an NVIDIA A100 GPU.

Performance on Non-homogeneous Haze. MITNet [58] and OKNet [10] are competitive in terms of PSNR and SSIM, respectively; however, our DehazeMatic achieves the highest performance in both metrics across all datasets. Moreover, as shown in Figure 6, MITNet [58] and OKNet [10] suffer from blue artifacts and blurred details, respectively. In contrast, DehazeMatic generates haze-free images with optimal fidelity and richer structural details while maintaining the highest quantitative scores.

Performance on Homogeneous Haze. DehazeMatic achieves the SOTA in the average performance of indoor and outdoor scenes, and especially significantly outperforms the second-best method by 0.79 dB with fewer MACs in outdoor scenes. Figure 7 provides visual comparisons on the SOTS Indoor dataset [38]. In the green and red boxed regions, DehazeMatic exhibits superior color consistency and

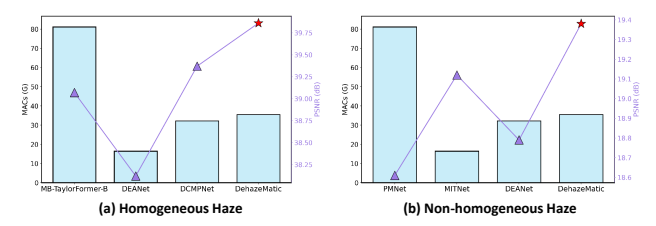


Figure 8. Illustration of trade-off between performance and overhead. The line chart in (a) represents the average PSNR on the SOTS-Indoor and SOTS-Outdoor datasets, while the line chart in (b) represents the average PSNR on the NH-Haze and Dense-Haze datasets. The greater the extent to which the line chart's value exceeds that of the bar chart, the better the model's trade-off.

effectively restores finer details, respectively.

Trade-off between Performance and Overhead. As shown in Figure 8, our DehazeMatic achieves the best trade-off for both types of haze, demonstrating its high efficiency. **Generalization on Real-world Haze Dataset.** To evaluate generalization, we compare DehazeMatic with several com-

Table 2. Quantitative comparisons of various methods on real-world haze dataset RTTS [38]. The best results and the second best results are in **bold** and <u>underline</u>, respectively.

No-reference Metrics	FFA-Net	MB-TaylorFormer-B	MITNet	DehazeFormer	DEA-Net	OKNet	DCMPNet	DehazaMatic
PIQE↓	48.199	30.248	52.685	48.230	48.889	31.742	33.576	28.123
BRISQUE↓	34.413	22.179	36.171	34.217	32.025	24.683	<u>21.374</u>	20.573
ENTROPY ↑	<u>7.164</u>	6.907	7.080	7.090	7.079	7.112	7.143	7.405

Table 3. Ablation study of the explicit coexistence of short- and long-range dependencies.

Setting	SOTS-	Indoor	NH-Haze		
Setting	PSNR↑	SSIM↑	PSNR↑	SSIM↑	
Only Short Dependencies	38.41	0.992	20.40	0.771	
Only Long Dependencies	39.78	0.994	20.56	0.779	
DehazeMatic	41.50	0.996	21.47	0.806	
Only Convolution	38.29	0.992	20.33	0.767	
Only Linear Attention	40.06	0.994	20.65	0.780	
Conv. & Linear Attention	41.41	0.996	21.36	0.803	

Table 4. Ablation study of CLIP-enhanced Dual-path Aggregator.

Set	ting	SOTS-	Indoor	NH-Haze		
		PSNR↑	SSIM↑	PSNR↑	SSIM↑	
(a) Remove CedA	Addition	39.55	0.993	20.71	0.781	
	Concatenation	39.80	0.994	20.74	0.784	
(b) Overall Design	W/o Density Map	40.88	0.995	20.91	0.792	
	W/o Semantic Map	41.02	0.995	21.23	0.794	
	Transmission Map	40.97	0.995	21.27	0.797	
(c) Density Map	Depth Map	41.16	0.996	21.28	0.795	
	Predefined Prompts	40.24	0.994	20.82	0.789	
(d) Comotio Mon	W/o High-level	41.12	0.995	21.30	0.800	
(d) Sematic Map	W/o Low-level	41.19	0.996	21.34	0.802	
Dehaz	41.50	0.996	21.47	0.806		

petitive methods on the real-world haze dataset RTTS [38], using models trained on the RESIDE OTS dataset [38] for inference. As shown in Table 2, our method outperforms all others across no-reference metrics, highlighting its superior generalization ability and practical applicability.

4.3. Ablation Studies

We conduct extensive ablation studies to demonstrate the effectiveness of each component. For a fair comparison, we tune the hyperparameters of variant models to ensure that their overhead matches that of DehazeMatic.

Explicit Coexistence of Short- and Long-range Dependencies. We remove either the Mamba path (*i.e.*, long-range) or the Transformer path (*i.e.*, short-range) in the TrambaDA blocks to construct variant models, while simultaneously excluding the CedA module. The corresponding results are shown in the first three rows of Table 3.

Additionally, to verify that its superiority is not de-

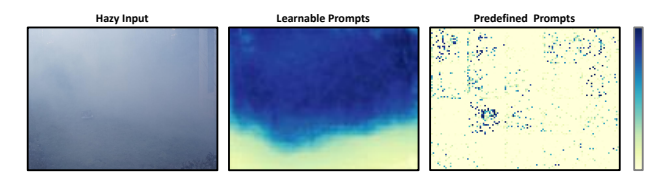


Figure 9. Visual comparisons of haze density maps estimated using learned prompts and manually predefined prompts.

pendent on a specific feature extractor, we use convolution [78] (*i.e.*, short-range), linear self-attention [51] (*i.e.*, long-range) and the proposed CedA module to construct a variant model and repeat the above experiments. The corresponding quantitative results are presented in the last three rows of Table 3, demonstrating the versatility of our idea. Although linear self-attention [51] achieves better results than the adopted Mamba block, its time cost is significantly larger, so we do not adopt it. The comprehensive results in Table 3 demonstrate that the complementary short- and long-range dependencies introduced by the dual-path design, along with their reasonable aggregation, can significantly enhance image dehazing.

CLIP-enhanced Dual-path Aggregator (CedA). As shown in Table 4, we conduct extensive ablation studies on the CedA to verify the effectiveness of each component.

- (a) We replace the CedA with addition and concatenation operations to verify the necessity of adaptively aggregating short- and long-range dependencies in the dual paths.
- (b) We then verify the importance of jointly using haze density and semantic information for aggregation guidance by removing each component individually.
- (c) Next, we investigate the estimated haze density map. First, we verify the rationale for using the density map rather than other commonly used guidance signals in dehazing (i.e., the transmission map from DCP [22] and the depth map from Depth Anything [67]) to guide the aggregation. The results indicate that haze density is a more suitable influencing factor.

Furthermore, we use manually predefined prompts to estimate the haze density map to verify the effectiveness of using learnable prompts. As shown in Table 4, predefined prompts lead to a significant performance drop, even falling behind the approach that relies solely on semantic maps for aggregation guidance. In addition, as illustrated in Figure 9, predefined prompts are entirely incapable of generat-

ing valid patch-wise haze density map.

(*d*) Finally, we validate the necessity of each type of information in the refined semantic map by ablating either high-level semantic information (*i.e.*, from CLIP) or low-level semantic information (*i.e.*, input of Tramba blocks).

5. Conclusion

In this paper, we propose DehazeMatic, a framework that employs a dual-path design to explicitly and simultaneously capture complementary local fine-grained details and global contextual cues. Based on key insights from our experiments—namely that different tokens in an image require varying ranges of dependencies and that haze density and semantic information are the primary factors influencing the required range—we introduce the CLIP-enhanced Dual-path Aggregator. It leverages the rich semantic priors and powerful generalization ability encapsulated in CLIP to ensure that each dependency contributes optimally to performance while further exploring CLIP's potential in image dehazing. Extensive experiments demonstrate that Dehaze-Matic outperforms SOTA methods on various benchmarks and holds promise for inspiring future research.

References

- [1] Yuang Ai, Huaibo Huang, Xiaoqiang Zhou, Jiexiang Wang, and Ran He. Multimodal prompt perceiver: Empower adaptiveness generalizability and fidelity for all-in-one image restoration. In <u>Proceedings of the IEEE/CVF Conference on Computer Vision and Pattern Recognition</u>, pages 25432–25444, 2024.
- [2] Codruta O Ancuti, Cosmin Ancuti, Mateu Sbert, and Radu Timofte. Dense-haze: A benchmark for image dehazing with dense-haze and haze-free images. In 2019 IEEE international conference on image processing (ICIP), pages 1014–1018. IEEE, 2019.
- [3] Codruta O Ancuti, Cosmin Ancuti, and Radu Timofte. Nh-haze: An image dehazing benchmark with nonhomogeneous hazy and haze-free images. In <u>Proc. Conf.</u> <u>Comput. Vis. Pattern Recognit. workshops</u>, pages 444–445, 2020.
- [4] Dylan Auty and Krystian Mikolajczyk. Learning to prompt clip for monocular depth estimation: Exploring the limits of human language. In <u>Proceedings of the IEEE/CVF</u> <u>International Conference on Computer Vision</u>, pages 2039– 2047, 2023.
- [5] Haoran Bai, Jinshan Pan, Xinguang Xiang, and Jinhui Tang. Self-guided image dehazing using progressive feature fusion. IEEE Trans. Image Process., 31:1217–1229, 2022.
- [6] Dana Berman, Tali Treibitz, and Shai Avidan. Single image dehazing using haze-lines. <u>IEEE transactions on pattern analysis and machine intelligence</u>, 42(3):720–734, 2018.
- [7] Bolun Cai, Xiangmin Xu, Kui Jia, Chunmei Qing, and Dacheng Tao. Dehazenet: An end-to-end system for single image haze removal. <u>IEEE Trans. Image Process.</u>, 25(11):5187–5198, 2016.

- [8] Zixuan Chen, Zewei He, and Zhe-Ming Lu. Dea-net: Single image dehazing based on detail-enhanced convolution and content-guided attention. <u>IEEE Transactions on Image</u> Processing, 2024.
- [9] Xiaofeng Cong, Jie Gui, Jing Zhang, Junming Hou, and Hao Shen. A semi-supervised nighttime dehazing baseline with spatial-frequency aware and realistic brightness constraint. In Proceedings of the IEEE/CVF Conference on Computer Vision and Pattern Recognition, pages 2631–2640, 2024.
- [10] Yuning Cui, Wenqi Ren, and Alois Knoll. Omni-kernel network for image restoration. In <u>Proceedings of the AAAI</u> <u>Conference on Artificial Intelligence</u>, volume 38, pages 1426–1434, 2024.
- [11] Yuning Cui, Qiang Wang, Chaopeng Li, Wenqi Ren, and Alois Knoll. Eenet: An effective and efficient network for single image dehazing. <u>Pattern Recognition</u>, 158:111074, 2025.
- [12] Soham De and Sam Smith. Batch normalization biases residual blocks towards the identity function in deep networks. <u>Advances in Neural Information Processing Systems</u>, 33:19964–19975, 2020.
- [13] Hang Dong, Jinshan Pan, Lei Xiang, Zhe Hu, Xinyi Zhang, Fei Wang, and Ming-Hsuan Yang. Multi-scale boosted dehazing network with dense feature fusion. In <u>Proc. Conf.</u> Comput. Vis. Pattern Recognit., pages 2157–2167, 2020.
- [14] Alexey Dosovitskiy. An image is worth 16x16 words: Transformers for image recognition at scale. <u>arXiv preprint</u> arXiv:2010.11929, 2020.
- [15] Wenxuan Fang, Jankai Fan, Yu Zheng, Jiangwei Weng, Ying Tai, and Jun Li. Guided real image dehazing using ycbcr color space. arXiv preprint arXiv:2412.17496, 2024.
- [16] Raanan Fattal. Single image dehazing. <u>ACM transactions on graphics</u> (TOG), 27(3):1–9, 2008.
- [17] Yuxin Feng, Long Ma, Xiaozhe Meng, Fan Zhou, Risheng Liu, and Zhuo Su. Advancing real-world image dehazing: Perspective, modules, and training. <u>IEEE Transactions on</u> Pattern Analysis and Machine Intelligence, 2024.
- [18] Albert Gu and Tri Dao. Mamba: Linear-time sequence modeling with selective state spaces. <u>arXiv preprint</u> arXiv:2312.00752, 2023.
- [19] Albert Gu, Karan Goel, and Christopher Ré. Efficiently modeling long sequences with structured state spaces. <u>arXiv</u> preprint arXiv:2111.00396, 2021.
- [20] Chun-Le Guo, Qixin Yan, Saeed Anwar, Runmin Cong, Wenqi Ren, and Chongyi Li. Image dehazing transformer with transmission-aware 3d position embedding. In <u>Proceedings of the IEEE/CVF conference on computer</u> vision and pattern recognition, pages 5812–5820, 2022.
- [21] Yu Guo, Yuan Gao, Wen Liu, Yuxu Lu, Jingxiang Qu, Shengfeng He, and Wenqi Ren. Scanet: Self-paced semicurricular attention network for non-homogeneous image dehazing. In Proceedings of the IEEE/CVF Conference on Computer Vision and Pattern Recognition, pages 1885– 1894, 2023.
- [22] Kaiming He, Jian Sun, and Xiaoou Tang. Single image haze removal using dark channel prior. <u>IEEE transactions on pattern analysis and machine intelligence</u>, 33(12):2341–2353, 2010.

- [23] Kaiming He, Xiangyu Zhang, Shaoqing Ren, and Jian Sun. Deep residual learning for image recognition. In <u>Proceedings</u> of the IEEE conference on computer vision and pattern recognition, pages 770–778, 2016.
- [24] Xueting Hu, Ce Zhang, Yi Zhang, Bowen Hai, Ke Yu, and Zhihai He. Learning to adapt clip for few-shot monocular depth estimation. In <u>Proceedings of the IEEE/CVF</u> <u>Winter Conference on Applications of Computer Vision</u>, pages 5594–5603, 2024.
- [25] Tao Huang, Xiaohuan Pei, Shan You, Fei Wang, Chen Qian, and Chang Xu. Localmamba: Visual state space model with windowed selective scan. <u>arXiv preprint arXiv:2403.09338</u>, 2024.
- [26] Gabriel Ilharco, Mitchell Wortsman, Ross Wightman, Cade Gordon, Nicholas Carlini, Rohan Taori, Achal Dave, Vaishaal Shankar, Hongseok Namkoong, John Miller, Hannaneh Hajishirzi, Ali Farhadi, and Ludwig Schmidt. Openclip, July 2021. If you use this software, please cite it as below.
- [27] Yitong Jiang, Zhaoyang Zhang, Tianfan Xue, and Jinwei Gu. Autodir: Automatic all-in-one image restoration with latent diffusion. In <u>European Conference on Computer Vision</u>, pages 340–359. Springer, 2025.
- [28] Yeying Jin, Wending Yan, Wenhan Yang, and Robby T Tan. Structure representation network and uncertainty feedback learning for dense non-uniform fog removal. In <u>Asian</u> <u>Conference on Computer Vision</u>, pages 155–172. Springer, 2022.
- [29] Justin Johnson, Alexandre Alahi, and Li Fei-Fei. Perceptual losses for real-time style transfer and super-resolution. In Computer Vision–ECCV 2016: 14th European Conference, Amsterdam, The Netherlands, October 11-14, 2016, Proceedings, Part II 14, pages 694–711. Springer, 2016.
- [30] Bum Jun Kim, Hyeyeon Choi, Hyeonah Jang, Dong Gu Lee, Wonseok Jeong, and Sang Woo Kim. Dead pixel test using effective receptive field. <u>Pattern Recognition Letters</u>, 167:149–156, 2023.
- [31] Se Eun Kim, Tae Hee Park, and Il Kyu Eom. Fast single image dehazing using saturation based transmission map estimation. <u>IEEE Transactions on Image Processing</u>, 29:1985–1998, 2019.
- [32] Diederik P Kingma and Jimmy Ba. Adam: A method for stochastic optimization. <u>arXiv preprint arXiv:1412.6980</u>, 2014.
- [33] Alex Krizhevsky, Ilya Sutskever, and Geoffrey E Hinton. Imagenet classification with deep convolutional neural networks. <u>Advances in neural information processing systems</u>, 25, 2012.
- [34] Ashutosh Kulkarni and Subrahmanyam Murala. Aerial image dehazing with attentive deformable transformers. In Proceedings of the IEEE/CVF Winter Conference on Applications of Computer Vision, pages 6305–6314, 2023.
- [35] Ashutosh Kulkarni, Shruti S Phutke, and Subrahmanyam Murala. Unified transformer network for multi-weather image restoration. In <u>European Conference on Computer</u> <u>Vision</u>, pages 344–360. Springer, 2022.

- [36] Boyun Li, Yuanbiao Gou, Jerry Zitao Liu, Hongyuan Zhu, Joey Tianyi Zhou, and Xi Peng. Zero-shot image dehazing. IEEE Transactions on Image Processing, 29:8457–8466, 2020.
- [37] Boyi Li, Xiulian Peng, Zhangyang Wang, Jizheng Xu, and Dan Feng. Aod-net: All-in-one dehazing network. In <u>Proc.</u> IEEE. Int. Conf. Comput. Vis., pages 4770–4778, 2017.
- [38] Boyi Li, Wenqi Ren, Dengpan Fu, Dacheng Tao, Dan Feng, Wenjun Zeng, and Zhangyang Wang. Benchmarking singleimage dehazing and beyond. <u>IEEE Trans. Image Process.</u>, 28(1):492–505, 2018.
- [39] Chengyang Li, Heng Zhou, Yang Liu, Caidong Yang, Yongqiang Xie, Zhongbo Li, and Liping Zhu. Detectionfriendly dehazing: Object detection in real-world hazy scenes. <u>IEEE Transactions on Pattern Analysis and Machine</u> Intelligence, 45(7):8284–8295, 2023.
- [40] Lerenhan Li, Yunlong Dong, Wenqi Ren, Jinshan Pan, Changxin Gao, Nong Sang, and Ming-Hsuan Yang. Semisupervised image dehazing. <u>IEEE Transactions on Image</u> Processing, 29:2766–2779, 2019.
- [41] Zhexin Liang, Chongyi Li, Shangchen Zhou, Ruicheng Feng, and Chen Change Loy. Iterative prompt learning for unsupervised backlit image enhancement. In <u>Proceedings</u> of the IEEE/CVF International Conference on Computer Vision, pages 8094–8103, 2023.
- [42] Jiarun Liu, Hao Yang, Hong-Yu Zhou, Yan Xi, Lequan Yu, Yizhou Yu, Yong Liang, Guangming Shi, Shaoting Zhang, Hairong Zheng, et al. Swin-umamba: Mambabased unet with imagenet-based pretraining. <u>arXiv preprint</u> arXiv:2402.03302, 2024.
- [43] Xiaohong Liu, Yongrui Ma, Zhihao Shi, and Jun Chen. Grid-dehazenet: Attention-based multi-scale network for image dehazing. In <u>Proceedings of the IEEE/CVF international conference on computer vision</u>, pages 7314–7323, 2019.
- [44] Yue Liu, Yunjie Tian, Yuzhong Zhao, Hongtian Yu, Lingxi Xie, Yaowei Wang, Qixiang Ye, and Yunfan Liu. Vmamba: Visual state space model. <u>arXiv preprint arXiv:2401.10166</u>, 2024.
- [45] Ze Liu, Yutong Lin, Yue Cao, Han Hu, Yixuan Wei, Zheng Zhang, Stephen Lin, and Baining Guo. Swin transformer: Hierarchical vision transformer using shifted windows. In Proceedings of the IEEE/CVF international conference on computer vision, pages 10012–10022, 2021.
- [46] Ilya Loshchilov and Frank Hutter. Sgdr: Stochastic gradient descent with warm restarts. arXiv:1608.03983, 2016.
- [47] Ziwei Luo, Fredrik K Gustafsson, Zheng Zhao, Jens Sjölund, and Thomas B Schön. Controlling vision-language models for universal image restoration. <u>arXiv preprint</u> arXiv:2310.01018, 2023.
- [48] Igor Morawski, Kai He, Shusil Dangi, and Winston H Hsu. Unsupervised image prior via prompt learning and clip semantic guidance for low-light image enhancement. In Proceedings of the IEEE/CVF Conference on Computer Vision and Pattern Recognition, pages 5971–5981, 2024.
- [49] Srinivasa G Narasimhan and Shree K Nayar. Vision and the atmosphere. <u>International journal of computer vision</u>, 48:233–254, 2002.

- [50] Xu Qin, Zhilin Wang, Yuanchao Bai, Xiaodong Xie, and Huizhu Jia. Ffa-net: Feature fusion attention network for single image dehazing. In <u>Proceedings of the AAAI conference</u> on artificial intelligence, volume 34, pages 11908–11915, 2020.
- [51] Yuwei Qiu, Kaihao Zhang, Chenxi Wang, Wenhan Luo, Hongdong Li, and Zhi Jin. Mb-taylorformer: Multi-branch efficient transformer expanded by taylor formula for image dehazing. In <u>Proceedings of the IEEE/CVF International</u> Conference on Computer Vision, pages 12802–12813, 2023.
- [52] Alec Radford, Jong Wook Kim, Chris Hallacy, Aditya Ramesh, Gabriel Goh, Sandhini Agarwal, Girish Sastry, Amanda Askell, Pamela Mishkin, Jack Clark, et al. Learning transferable visual models from natural language supervision. In International conference on machine learning, pages 8748–8763. PMLR, 2021.
- [53] Jingjing Ren, Haoyu Chen, Tian Ye, Hongtao Wu, and Lei Zhu. Triplane-smoothed video dehazing with clip-enhanced generalization. <u>International Journal of Computer Vision</u>, pages 1–14, 2024.
- [54] Wenqi Ren, Si Liu, Hua Zhang, Jinshan Pan, Xiaochun Cao, and Ming-Hsuan Yang. Single image dehazing via multi-scale convolutional neural networks. In Computer Vision–ECCV 2016: 14th European Conference, Amsterdam, The Netherlands, October 11-14, 2016, Proceedings, Part II 14, pages 154–169. Springer, 2016.
- [55] Wenqi Ren, Lin Ma, Jiawei Zhang, Jinshan Pan, Xiaochun Cao, Wei Liu, and Ming-Hsuan Yang. Gated fusion network for single image dehazing. In Proc. Conf. Comput. Vis. Pattern Recognit., pages 3253–3261, 2018.
- [56] Wenqi Ren, Jinshan Pan, Hua Zhang, Xiaochun Cao, and Ming-Hsuan Yang. Single image dehazing via multi-scale convolutional neural networks with holistic edges. <u>Int. J.</u> Comput. Vis., 128(1):240–259, 2020.
- [57] Yuanjie Shao, Lerenhan Li, Wenqi Ren, Changxin Gao, and Nong Sang. Domain adaptation for image dehazing. In <u>Proceedings of the IEEE/CVF conference on computer vision and pattern recognition</u>, pages 2808–2817, 2020.
- [58] Hao Shen, Zhong-Qiu Zhao, Yulun Zhang, and Zhao Zhang. Mutual information-driven triple interaction network for efficient image dehazing. In <u>Proceedings of the 31st ACM</u> International Conference on Multimedia, pages 7–16, 2023.
- [59] Yuda Song, Zhuqing He, Hui Qian, and Xin Du. Vision transformers for single image dehazing. <u>IEEE Transactions on Image Processing</u>, 32:1927–1941, 2023.
- [60] Robby T Tan. Visibility in bad weather from a single image. In 2008 IEEE conference on computer vision and pattern recognition, pages 1–8. IEEE, 2008.
- [61] Zhengzhong Tu, Hossein Talebi, Han Zhang, Feng Yang, Peyman Milanfar, Alan Bovik, and Yinxiao Li. Maxim: Multi-axis mlp for image processing. In Proceedings of the IEEE/CVF conference on computer vision and pattern recognition, pages 5769–5780, 2022.
- [62] Andreas Veit, Michael J Wilber, and Serge Belongie. Residual networks behave like ensembles of relatively shallow networks. Advances in neural information processing systems, 29, 2016.

- [63] Ruiyi Wang, Wenhao Li, Xiaohong Liu, Chunyi Li, Zicheng Zhang, Xiongkuo Min, and Guangtao Zhai. Hazeclip: Towards language guided real-world image dehazing. <u>arXiv</u> preprint arXiv:2407.13719, 2024.
- [64] Yongzhen Wang, Jiamei Xiong, Xuefeng Yan, and Mingqiang Wei. Uscformer: unified transformer with semantically contrastive learning for image dehazing. <u>IEEE</u> Transactions on Intelligent Transportation Systems, 2023.
- [65] Zhongze Wang, Haitao Zhao, Jingchao Peng, Lujian Yao, and Kaijie Zhao. Odcr: Orthogonal decoupling contrastive regularization for unpaired image dehazing. In <u>Proceedings of the IEEE/CVF Conference on Computer Vision and Pattern Recognition</u>, pages 25479–25489, 2024.
- [66] Haiyan Wu, Yanyun Qu, Shaohui Lin, Jian Zhou, Ruizhi Qiao, Zhizhong Zhang, Yuan Xie, and Lizhuang Ma. Contrastive learning for compact single image dehazing. In Proc. IEEE/CVF Conf. Comput. Vis. Pattern Recognit., pages 10551–10560, 2021.
- [67] Lihe Yang, Bingyi Kang, Zilong Huang, Xiaogang Xu, Jiashi Feng, and Hengshuang Zhao. Depth anything: Unleashing the power of large-scale unlabeled data. In <u>Proceedings of</u> the IEEE/CVF Conference on Computer Vision and Pattern Recognition, pages 10371–10381, 2024.
- [68] Yang Yang, Chaoyue Wang, Xiaojie Guo, and Dacheng Tao. Robust unpaired image dehazing via density and depth decomposition. <u>International Journal of Computer Vision</u>, 132(5):1557–1577, 2024.
- [69] Zizheng Yang, Hu Yu, Bing Li, Jinghao Zhang, Jie Huang, and Feng Zhao. Unleashing the potential of the semantic latent space in diffusion models for image dehazing. In European Conference on Computer Vision, pages 371–389. Springer, 2025.
- [70] Tian Ye, Yunchen Zhang, Mingchao Jiang, Liang Chen, Yun Liu, Sixiang Chen, and Erkang Chen. Perceiving and modeling density for image dehazing. In <u>European conference on computer vision</u>, pages 130–145. Springer, 2022.
- [71] Hu Yu, Naishan Zheng, Man Zhou, Jie Huang, Zeyu Xiao, and Feng Zhao. Frequency and spatial dual guidance for image dehazing. In European Conference on Computer Vision, pages 181–198. Springer, 2022.
- [72] He Zhang and Vishal M Patel. Densely connected pyramid dehazing network. In Proc. Conf. Comput. Vis. Pattern Recognit., pages 3194–3203, 2018.
- [73] Ruikun Zhang, Hao Yang, Yan Yang, Ying Fu, and Liyuan Pan. Lmhaze: Intensity-aware image dehazing with a largescale multi-intensity real haze dataset. In Proceedings of the 6th ACM International Conference on Multimedia in Asia, pages 1–1, 2024.
- [74] Renrui Zhang, Ziyao Zeng, Ziyu Guo, and Yafeng Li. Can language understand depth? In Proceedings of the 30th ACM <u>International Conference on Multimedia</u>, pages 6868–6874, 2022.
- [75] Xiaoqin Zhang, Tao Wang, Jinxin Wang, Guiying Tang, and Li Zhao. Pyramid channel-based feature attention network for image dehazing. <u>Comput. Vis. Image Understanding</u>, 197:103003, 2020.

- [76] Yi Zhang, Meng-Hao Guo, Miao Wang, and Shi-Min Hu. Exploring regional clues in clip for zero-shot semantic segmentation. In Proceedings of the IEEE/CVF Conference on Computer Vision and Pattern Recognition, pages 3270–3280, 2024.
- [77] Yafei Zhang, Shen Zhou, and Huafeng Li. Depth information assisted collaborative mutual promotion network for single image dehazing. In Proceedings of the IEEE/CVF Conference on Computer Vision and Pattern Recognition, pages 2846–2855, 2024.
- [78] Yu Zheng, Jiahui Zhan, Shengfeng He, Junyu Dong, and Yong Du. Curricular contrastive regularization for physics-aware single image dehazing. In <u>Proceedings of the IEEE/CVF conference on computer vision and pattern recognition</u>, pages 5785–5794, 2023.
- [79] Zhuoran Zheng and Chen Wu. U-shaped vision mamba for single image dehazing. <u>arXiv preprint arXiv:2402.04139</u>, 2024.
- [80] Huiling Zhou, Xianhao Wu, Hongming Chen, Xiang Chen, and Xin He. Rsdehamba: Lightweight vision mamba for remote sensing satellite image dehazing. <u>arXiv:2405.10030</u>, 2024.
- [81] Ziqin Zhou, Yinjie Lei, Bowen Zhang, Lingqiao Liu, and Yifan Liu. Zegclip: Towards adapting clip for zero-shot semantic segmentation. In Proceedings of the IEEE/CVF Conference on Computer Vision and Pattern Recognition, pages 11175–11185, 2023.
- [82] Lianghui Zhu, Bencheng Liao, Qian Zhang, Xinlong Wang, Wenyu Liu, and Xinggang Wang. Vision mamba: Efficient visual representation learning with bidirectional state space model. arXiv preprint arXiv:2401.09417, 2024.
- [83] Qingsong Zhu, Jiaming Mai, and Ling Shao. A fast single image haze removal algorithm using color attenuation prior. <u>IEEE transactions on image processing</u>, 24(11):3522–3533, 2015.